Proceedings of Dynamic Systems and Applications 5 (2008) 240-246

MODELS OF PHOTOTRANSDUCTION IN ROD PHOTORECEPTORS

HARIHAR KHANAL[1] AND VASILIOS ALEXIADES[2]

[1] Department of Mathematics, Embry-Riddle Aeronautical University, Daytona Beach FL 32114
[2] Department of Mathematics, University of Tennessee, Knoxville TN 37996
and Oak Ridge National Laboratory, Oak Ridge TN 37831

ABSTRACT. Phototransduction is the process by which photons of light generate an electrical response in retinal rod and cone photoreceptors, thereby initiating vision. We compare the electrical response in salamander rods from increasingly more (spacialy) detailed models of phototransduction: 0-dimensional (bulk), 1-dimensional (longitudinal), 2-dimensional (axisymmetric), and 3-dimensional (with incisures). We discuss issues of finding physical parameters for simulation and validation of models, and also present some computational experiments for rods with geometry of mouse and human photoreceptors.

AMS (MOS) Subject Classification. 92C45, 35K60, 65M99.

1. INTRODUCTION

Phototransduction in rod photoreceptors is among the best understood biological signaling processes, with the underlying biochemistry, geometry and physiology of the rod outer segment (ROS) known in fair detail.

Traditionally, the basic signaling processes are investigated in terms of bulk quantities using Michaelis-Menten type kinetics (Pugh & Lamb, 2000) resulting in ordinary differential equations for the averaged concentrations within the volume of the ROS. However, signaling molecules reside at specific sites within cells or their plasma membrane; to analyse the regulation process quantitatively, it is necessary to take into account the local concentrations and time-dependent diffusion. Great strides have been made recently in developing spatio–temporal models (Andreucci et al., 2003; Khanal et al., 2003; Khanal et al. 2004; Caruso et al. 2005; Caruso et al. 2006; Alexiades & Khanal, 2007), extending previous bulk models of (Lamb & Pugh, 1992; Nikonov et al., 2000; Pugh & Lamb, 2000). The model in (Caruso et al. 2005; Alexiades & Khanal, 2007) incorporates all the mechanisms presently known to operate in rod phototransduction, and it reduces to simpler models proposed by physiologists, as described in §3 below. Some facts concerning the spread of a single photon response (SPR) (Gray-Keller et al., 1999; Lamb et al., 1992) have been tested numerically and the process of determining a consistent set of parameters for salamander rods began (Khanal et al., 2003; Khanal et al. 2004; Caruso et al. 2005). The currently available experimental data do not capture the spatial complexity of the linked diffusion of cGMP and $Ca^{2+}$and there is no general agreement for values for some of these parameters in the literature. Thus, the issue of determining a consistent set of parameters is paramount.

In this paper, we compare single-photon responses generated by a sequence of increasingly more (spatialy) detailed models, namely: 0-dimensional (bulk), 1-dimensional (longitudinal), 2-dimensional (axisymmetric), and 3-dimensional (with incisures). Analyzing simulation results from these models we find that the amplitude of response can be controlled by a single activation parameter, namely $\nu_{\rm RE}$ (see Eq. (3.7)). In our comparison, we considered the axially symmetric 2-D model as a reference solution since it has been validated with experimental data (Caruso et al. 2005). We determine values of $\nu_{\rm RE}$ such that the longitudinal and the bulk models yield the same peak response as the validated 2-D model. Finally, simulation results for rods having the geometry of mouse and human photoreceptors are presented and compared with that of salamander.

The organization of the remaining sections is as follows. After a brief description of the phototransduction process in §2, the mathematical models are outlined in §3. Simulations and their significance are described in §4, and conclusions in §5.

2. PHOTOTRANSDUCTION

The first stage of vision occurs in photoreceptor cells in the back of the retina, which capture light and produce an electrical response. Rod photoreceptors contain a stack of (about 1000) "discs" (bilipid membranes) with embedded

rhodopsin molecules, which absorb the photons and trigger a complex biochemical cascade (Hamer et al., 2003; Alexiades, 2007) resulting in production of activated phosphodiesterase (PDE*). This depletes cyclic guanosine monophosphate (cGMP) in the cytosol of the rod outer segment (ROS). The plasma membrane of the ROS contains cGMP–gated channels, which are open in darkness, permitting influx of Na^+ and Ca^{2+} ions; a steady *dark* current is maintained by the $Na^+/K^+/Ca^{2+}$exchanger mechanism. Depletion of cGMP causes local closing of channels, thus lowering the local current across the plasma membrane. This is the signal that eventually reaches the brain enabling vision. A Ca^{2+}–mediated feedback mechanism deactivates rhodopsin and increases cGMP production, thus reopening the channels and restoring the dark current. We refer to (Pugh & Lamb, 2000) for a detailed description of phototransduction. Sensitivity analysis and parameter optimization of the biochemical cascade on discs via the bulk model is presented in (Alexiades, 2007). The essential players in the process are PDE*, produced on the discs, and the second messengers, cGMP and Ca^{2+}, which by diffusion in the cytosol carry the signal to and from the plasma membrane.

The mathematical model assumes a specified number of activated PDE subunits in the entire ROS, $E(t)$ (see Eq. (3.7)) and accounts for the diffusion of cGMP and $Ca^{2+}$and their interactions on disc surfaces and on the plasma membrane. The current, $J(t)$, across the plasma membrane can be found directly in terms of the boundary values of [cG] and [Ca], where [cG] and [Ca] denote concentrations of cGMP and Ca^{2+}at any time t (§3). We are interested in the cellular *response*, $J_{\text{dark}} - J(t)$, or rather in the *normalized response* $\mathfrak{R}(t) = 1 - J(t)/J_{\text{dark}}$, with J_{dark} the dark steady-state current (see Eq. (3.3)).

3. MATHEMATICAL MODELS

3.1. **Geometry.** The rod outer segment (ROS) of a photoreceptor in vertebrates can be considered as a circular cylinder of height H and radius R_{rod}, housing a vertical stack of N equispaced parallel discs $\mathcal{D}_j,\ j = 1, 2, \cdots N$, coaxial with the cylinder, each of radius R_{dsc}, and thickness ε. The distance between discs, and the gap $R_{rod} - R_{dsc}$, are also small, $\sim \varepsilon$. The region inside the ROS not occupied by the discs is filled with cytosol. This is the region Ω where diffusion of second messengers takes place. We denote by $F_j^{\pm}$ the upper/lower disc faces, and by $\partial_o\Omega$ the lateral outer boundary (plasma membrane).

In some animals, the discs have narrow radial cuts, called *incisures* (Caruso et al., 2006), which we simulate as a narrow sector cut out of the disc. The presence of incisures decreases the area A_{dsc} of disc faces, increases the cytosolic volume V_{cyt}, and enhances longitudinal diffusion. Moreover, it renders the process 3-dimensional, even when the activation term $[\text{PDE}^*]_s$ appearing in Eq. (3.2a) is uniform over the disc.

3.2. **3-D Model.** Employing cylindrical coordinates (r, z, θ), the mathematical model for the diffusion of cGMP and Ca^{2+}in cytosol is expressed as follows. Given $[\text{cG}](r, z, \theta, 0) = [\text{cG}]_{\text{init}}$, $[\text{Ca}](r, z, \theta, 0) = [\text{Ca}]_{\text{init}}$ (the initial uniform steady-state for the dark adapted system), find $[\text{cG}](r, z, \theta, t)$, $[\text{Ca}](r, z, \theta, t)$ for $t > 0$, such that

$$\frac{\partial[\text{cG}]}{\partial t} - \nabla\cdot(D_{\text{cG}}\,\nabla[\text{cG}]) = 0, \quad \frac{\partial[\text{Ca}]}{\partial t} - \nabla\cdot(D_{\text{Ca}}\,\nabla[\text{Ca}]) = 0, \text{ in } \Omega, \text{ for } t > 0, \tag{3.1}$$

where D_{cG} and D_{Ca} are the respective diffusion coefficients.

Consider a beam of photons hitting a disc $\mathcal{D}_{j_*}$ on one of its faces, say for example the lower one, $F_{j_*}^-$, at coordinate z_* along the axis of the ROS. Generation and removal of free cGMP in the cytoplasm occurs through binding phenomena on the upper and lower faces $F_j^{\pm}$ of each disc $\mathcal{D}_j$. Calcium enters or leaves the cytosol only through the plasma membrane $\partial_o\Omega$, (via the cGMP-gated channels and the electrogenic exchanger). Thus the two diffusion equations in Eq. (3.1) are coupled via the following nonlinear boundary conditions:

$$-D_{\text{cG}}\frac{\partial[\text{cG}]}{\partial z} = \pm\,\alpha([\text{Ca}])\,\eta \mp k_{\text{hyd}}\,[\text{PDE}]_s[\text{cG}] + \delta_{j0}\,k^*_{\text{hyd}}[\text{PDE}^*]_s\,[\text{cG}], \quad \text{on } F_j^{\pm}, \tag{3.2a}$$

$$-D_{\text{Ca}}\frac{\partial[\text{Ca}]}{\partial r} = \frac{1}{B_{\text{Ca}}\,\mathcal{F}\,\Sigma_{\text{rod}}}\left(J_{\text{ex}} - \frac{1}{2}\,f_{\text{Ca}}\,J_{\text{cG}}\right) \quad \text{on } \partial_o\Omega. \tag{3.2b}$$

Here $\alpha([\text{Ca}]) = \alpha_{min} + (\alpha_{max} - \alpha_{min})/(1 + ([\text{Ca}]/K_{\text{cyc}})^{m_c})$ is the rate of synthesis of cGMP by guanylyl cyclase, α_{min} and α_{max} are the minimum and maximum rate of synthesis, m_c is the experimental Hill's exponents, K_{cyc} is the Ca^{2+}concentration that achieves half maximum rate, $\eta = V_{\text{cyt}}/A_{\text{dsc}}$ is the ratio of the cytosolic volume to the surface area of all disc faces, $[\text{PDE}]_s$ is the surface density of PDE, assumed uniformly distributed on the entire area of the faces of

the disc(s), k_{hyd} is the catalytic rate of dark-activated PDE, k^*_{hyd} is the catalytic rate of the light-activated PDE*, B_{Ca} is the buffering power of the cytoplasm for calcium, $\mathcal{F}$ is the Faraday constant, Σ_{rod} is the surface area of the ROS, J_{ex} is the electrogenic current carried by the exchanger, f_{Ca} is the fraction of cGMP-activated current carried by Ca^{2+}, J_{cG} is the current carried by the cGMP-gated channel, and $\delta_{j0} = 1$ if $j = j_*$ (activated face), and zero otherwise.

The quantity $[\text{PDE}^*]_s$ represents the strength of PDE* - cGMP interaction, and thus the effect of activation by light (see Eq. (3.7) – (3.8) below). The fluxes on the remaining parts of the boundary of Ω, and along the incisure, are zero.

The local current J at a point of the plasma membrane (with local concentrations [cG], [Ca] at that point) is the sum of the cG-gated, J_{cG}, and exchanger, J_{ex}, circulating currents (Nikonov et al., 2000; Pugh & Lamb, 2000)

$$J = J_{\text{cG}} + J_{\text{ex}}\,, \quad \text{with} \quad J_{\text{cG}} = \frac{j_{\text{cG}}^{\max}}{1 + (K_{\text{cG}}/[\text{cG}])^{m_{\text{cG}}}} \quad \text{and} \quad J_{\text{ex}} = \frac{j_{\text{ex}}^{\text{sat}}}{1 + K_{\text{ex}}/[\text{Ca}]} \tag{3.3}$$

where $j_{\text{cG}}^{\max}$ is the maximal cG-gated current, $j_{\text{ex}}^{\text{sat}}$ is the saturation exchanger current, K_{ex} is the half-saturating Ca^{2+} concentration of the exchanger, K_{cG} is the half maximum constant for cGMP, and m_{cG} is Hill constant.

3.3. **2-D Model.** If incisures are absent, or their presence is ignored, and the activation term $[\text{PDE}^*]_s$ is uniform on the face of the activated disc, as in Eq. (3.7), then there is no dependence on the angle θ, and the process is axially symmetric, hence 2-dimensional.

3.4. **1-D (Longitudinal) Model.** A simplified, one-dimensional model along the longitudinal (z) direction can be obtained by assuming uniform spatial distribution in the radial (r) direction. Indeed, Eq. (3.2b) gives the flow rate of [Ca] per unit area of lateral ROS surface. Thus, integrating Eq. (3.2b) over the lateral surface Σ_{rod} of the rod outer segment, we obtain the total flow rate of [Ca] in the entire ROS, which must be considered as a source term. The resulting longitudinal model takes the following form:

$$\frac{\partial[\text{cG}]}{\partial t} - D_{\text{cG}}\frac{\partial^2[\text{cG}]}{\partial z^2} = 0, \tag{3.4a}$$

$$\frac{\partial[\text{Ca}]}{\partial t} - D_{\text{Ca}}\frac{\partial^2[\text{Ca}]}{\partial z^2} = \frac{1}{B_{\text{Ca}}\,\mathcal{F}\,V_{\text{cyt}}}\left(J_{\text{ex}} - \frac{1}{2}\,f_{\text{Ca}}\,J_{\text{cG}}\right), \tag{3.4b}$$

for $0 < z < H$ and $t > 0$, and the boundary conditions given by

$$-D_{\text{cG}}\frac{\partial[\text{cG}]}{\partial z} = 0 \quad \text{on} \ \{z = 0\} \cup \{z = H\}\,, \tag{3.5a}$$

$$-D_{\text{cG}}\frac{\partial[\text{cG}]}{\partial z} = \pm\,\alpha\,\eta \mp k_{\text{hyd}}\,[\text{PDE}]_s[\text{cG}] + \delta_j\,k^*_{\text{hyd}}[\text{PDE}^*]_s[\text{cG}], \quad \text{on} \ F_j^{\pm} \tag{3.5b}$$

$$-D_{\text{Ca}}\frac{\partial[\text{Ca}]}{\partial z} = 0 \quad \text{on} \ F_j^{\pm} \cup \{z = 0\} \cup \{z = H\}\,. \tag{3.5c}$$

Note that the the quantity V_{cyt} on the right side of Eq. (3.4b) comes from the conversion of the boundary source Eq. (3.2b) to a volume source.

3.5. **0-D (Bulk) Model.** The one-dimensional longitudinal model (3.4a)–(3.5c) reduces to the lumped model of (Nikonov et al., 2000; Pugh & Lamb, 2000) under the assumption of spatially uniform concentrations. The total flow rate of [cG] in the entire ROS, obtained by integrating Eq. (3.5b) over the surface of all the discs, becomes a source term for the rate of change of bulk [cG]. The rate of change of [Ca] is simply given by the source term in Eq. (3.4b). Thus, the bulk (ordinary differential equations) model obtained by further reduction of the one dimensional longitudinal model described above takes the form

$$\frac{d[\text{cG}]}{dt} = \alpha - \frac{1}{\eta}\left(k_{\text{hyd}}\,[\text{PDE}]_s + \delta_{i0}\,k^*_{\text{hyd}}[\text{PDE}^*]_s\right)[\text{cG}], \tag{3.6a}$$

$$\frac{d[\text{Ca}]}{dt} = \frac{1}{B_{\text{Ca}}\,\mathcal{F}\,V_{\text{cyt}}}\left(J_{\text{ex}} - \frac{1}{2}\,f_{\text{Ca}}\,J_{\text{cG}}\right). \tag{3.6b}$$

The total [Ca] flow rate is identical to that of (Nikonov et al., 2000) while the matching of the [cG] flow rate is shown in (Caruso et al., 2005).

Note that the bulk model contains minimal information about the geometry of the ROS; only the quantities $\eta = V_{\text{cyt}}/A_{\text{dsc}}$ and V_{cyt} enter. Thus, the bulk model is inadequate for capturing ROS-geometry effects like those studied in §4.4 below.

3.6. **Light Activation.** Light activation is embodied in the quantity $[\text{PDE}^*]_s$ appearing in (3.2a). The literature contains various attempts to describe such a quantity (Pugh & Lamb, 2000; Nikonov et al. 1998; Nikonov et al. 2000; Andreucci at al., 2003; Khanal et al., 2003; Khanal et al., 2004; Hamer et al., 2003; Alexiades, 2007). Here we consider a simple activation mechanism with a lumped model, by taking the surface density of activated PDE molecules as the total PDE^* in the ROS divided by the area A_{activ} of activated discs,

$$[\text{PDE}^*]_s(x,t) = \frac{1}{2}\,\text{E}^*(t)/A_{\text{activ}} \tag{3.7}$$

where $\text{E}^*(t)$ is the number of γ-subunits of PDE at time t in the entire ROS (PDE is considered activated when both of its γ-subunits have been removed). Following (Nikonov et al. 1998; Pugh & Lamb, 2000), the quantity $\text{E}^*(t)$ is approximated in terms of two first-order rate constants k_{R}, k_{E}, representing decay rates of activated rhodopsin R^* and PDE^*, as

$$\text{E}^*(t) = \Phi \cdot \left(\frac{\nu_{\text{RE}}}{k_{\text{R}} - k_{\text{E}}}\right)\left(e^{-k_{\text{E}}t} - e^{-k_{\text{R}}t}\right), \quad t > 0\,, \tag{3.8}$$

where Φ is the number of photoisomerisations per rod per flash, and ν_{RE} is the effective rate with which a single R^* triggers activation of PDE^*.

Since this activation method applies the source $[\text{PDE}^*]_s(x,t)$ uniformly on each activated disc, the process is axially symmetric, reducing the computation to 2-dimensional (in r, z coordinates), unless incisures are taken into account.

4. NUMERICAL SIMULATIONS

4.1. **Discretization and Parallelization.** We employ Finite Volume discretization in space and explicit-implicit time-stepping. The numerical codes are implemented in Fortran, with time-steps sufficiently small to ensure numerical stability.

Due to the intricate geometry of the cytosol, the spatio-temporal models involve very intensive computations demanding high performance computing. This was addressed by parallelization, via domain decomposition, for clusters of distributed memory multiprocessors, by assigning groups of disc units to different processors. The parallel implementation employs the MPI (Message Passing Interface) library, following the master/slaves paradigm in SIMD (Single Instruction Multiple Data) mode, where one processor acts as a master and the rest as slaves. The master loads I/O, distributes tasks to the slaves, controls and synchronizes the slaves, whereas the slaves all solve the same problem but on their own segment of the mesh, exchange boundary values with their neighbors, and send their output to the master.

4.2. **Simulation Setup.** Estimates for the geometric parameters N = number of discs in the ROS, R_{rod}= ROS radius, R_{dsc}= disc radius, ε= disc thickness, Z_f= half of the vertical space between discs (with lengths in μm), and the resulting H= height of ROS, V_{cyt}= volume of cytosol, and Vol= volume of ROS, for three species (Pugh & Lamb, 2000; Caruso et al., 2005; Carter-Dawson & LaVail, 1979; Fulton, 2007) are shown in Table 1.

TABLE 1. Geometric Parameters

ROS	N	$R_{\text{rod}}(\mu m)$	$R_{\text{dsc}}(\mu m)$	$\varepsilon(\mu m)$	$Z_f(\mu m)$	$H(\mu m)$	$V_{\text{cyt}}(\mu m^3)$	Vol (μm^3)
salamander	800	5.515	5.5	0.014	0.007	22.4	1076	2140
mouse	1000	0.622	0.61	0.012	0.006	24	15	29
human	2000	1.0	0.992	0.018	0.004	52	52	163

Simulations were performed for *salamander*, *mouse* and *human* photoreceptors with the geomeric parameters described above. The values of all biophysical parameters entering the model (D_{cG}, D_{Ca}, k_{hyd}, $[PDE]_s$, k^*_{hyd}, B_{Ca}, $\mathcal{F}$, α_{min}, α_{max}, m_c, K_{cyc}, j^{max}_{cG}, j^{sat}_{ex}, K_{cG}, K_{ex}, m_{cG}) were taken to be those found for salamander in (Caruso et al., 2005), since values appropriate for mouse and human are not known.

The initial state is the dark steady-state with concentrations found by solving the system Eq. (3.2a) –(3.2b) after setting the fluxes to zero, yielding $[\text{cG}]_{\text{dark}} = 3\,\mu\text{M}$, $[\text{Ca}]_{\text{dark}} = 0.66\,\mu\text{M}$, and $\text{J}_{\text{dark}} = 66$ pA.

For PDE*-activation, the lumped method described in §3 was employed with rate constants $\nu_{\text{RE}} = 195\ \text{s}^{-1}$, $k_{\text{E}} = 0.6\ \text{s}^{-1}$ and $k_{\text{R}} = 2.6\ \text{s}^{-1}$, and $\Phi = 1$, simulating response to a single photon.

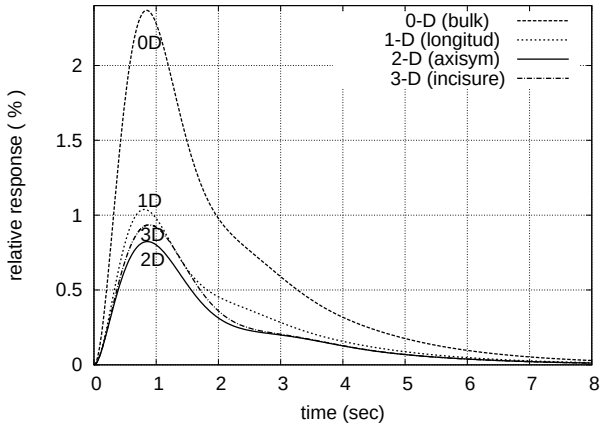

FIGURE 1. Relative response versus time for salamander with the same parameters in all four models.

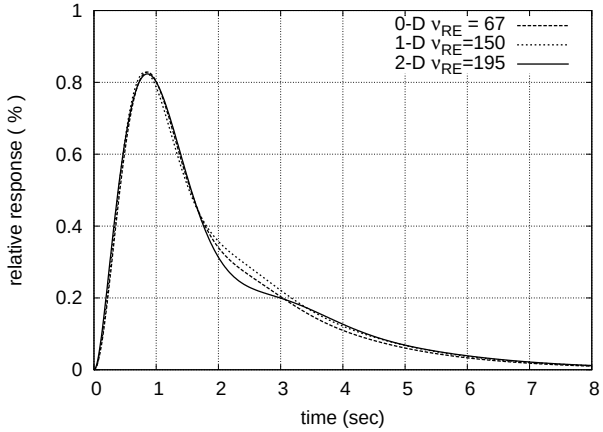

FIGURE 2. Simulations with 0-D, 1-D and 2-D models for salamander with $\nu_{\rm RE}$ adjusted to produce the same peak.

Computations were performed on a linux cluster at Embry-Riddle University (dual Intel Xeon 3.2GHz processors, 1024 KB cache, 4GB memory, with Myrinet MX, compiled with pgif90). Simulations presented here were run in a coarse mesh of 9 radial nodes, $4 \times N$ axial nodes for N discs and 5 angular nodes. Thus, for a ROS with N discs there are $4N$ control volumes in 1-D case, $9 \times 4 \times N = 36N$ in 2-D, and $9 \times 4 \times 5 \times N = 180N$ in 3-D. An 8 sec simulation with the 3-D code, for a typical salamander rod ($N = 800$ discs, incisure of area $0.82\,\mu m^2$), takes about 34 hrs of CPU time on 20 slave processors of the linux cluster at ERAU.

4.3. **Simulation Results.** Qualitatively, the models yield similar results, but quantitatively they do not agree in general. This is to be expected, since each of the models has its own limitations due to its simplifying assumptions, e.g., the ordinary differential equation model (Eq. (3.6a) – (3.6b)) assumes infinite diffusivities, the longitudinal (Eq. (3.4a) – (3.5c)) is diffusion limited in the axial direction only, and the full model (Eq. (3.1) – (3.2b)) is fully diffusion limited.

The response curves to a single photon ($\Phi = 1$ in Eq. (3.7)) stimulation for salamander rod photoreceptor from each of the models: bulk (0-D), longitudinal (1-D), axisymmetric (2-D) and incisures (3-D), all run with the same parameters, are presented in Fig. 1. The bulk model produces peak response 2.4%, three times higher than the 2-D model's 0.82%, with the 1-D at 1.04% and the full 3-D at 0.94%.

Comparing simulation results with various sets of parameter values, we found that the activation constant $\nu_{\rm RE}$, appearing in Eq. (3.7), regulates the response amplitude.

By lowering the value of $\nu_{\rm RE}$ from $195\,{\rm s}^{-1}$ to 67 for the 0-D and 150 for the 1-D, we obtain the same 0.82% peak from the 0-D, 1-D, and 2-D models, as seen in Fig. 2. The slightly higher peak of the 3-D model is due to the enhanced diffusion effect of the incisure.

4.4. **Effect of photoreceptor geometry.** Finally we consider the effect of geometric features, by comparing responses from rods having the geometry of a mouse and a human photoreceptor with that of salamander, shown in Fig. 3. The 2-D simulations used the same biochemical and light activation parameter values those for salamander, which have been validated against experimental data (Caruso et al., 2005), since such parameters for mouse and human are not known. Only the geometric parameters are different, as in Table 1. The thinnest ROS (mouse) yields a much stronger response,

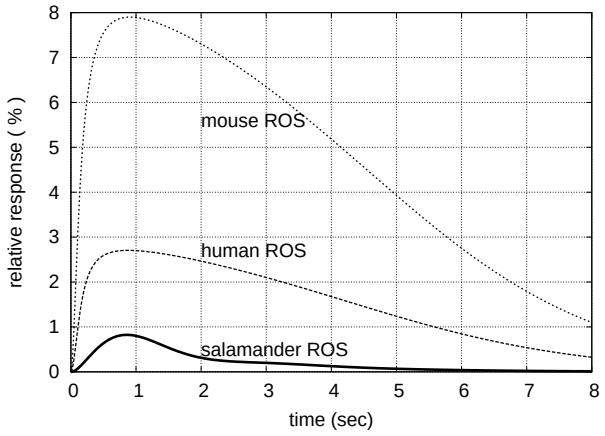

FIGURE 3. Comparison of response in salamander, mouse and human rods.

about 8%, than the wider human ROS, $\sim 2.7\%$, which in turn is much stronger than the 0.8% of the very wide salamander ROS. Note that the 1000-disc mouse ROS is 10 times thinner and generates 10 times higher response than the 800-disc salamander ROS. Simulations of an 800-disc ROS with mouse and human ROS geometries produce even higher peaks, 10% and 6.7% respectively.

Thus, the thinner the ROS the higher the response, and the higher the number of discs the lower the response. Clearly, photoreceptor geometry has a profound effect on response amplitude.

On the other hand, time-to-peak is about 900 ms for all of them, revealing its insensitivity to geometric features. Only the space-resolved 2-D and 3-D models can capture such effects.

Simulations are summarized in Table 2. For each animal and model, the table lists the mesh size and value of ν_{RE} used, the resulting peak response and time it occurs, as well as CPU timing and number of processors used.

TABLE 2. Summary of simulations with various models and geometries.

Species	Model	Mesh	$\nu_{\mathrm{RE}}(\mathrm{s}^{-1})$	Peak response%	time(ms)	CPU(h:m)	# Processor
salamander	0-D	–	67	0.82	860	–	1
	1-D	4×800	150	0.82	820	01:10	10
	2-D	$9 \times 4 \times 800$	195	0.82	860	03:04	10
	3-D	$9{\times}4{\times}5{\times}800$	195	0.94	890	34:26	20
mouse	2-D	$9 \times 4 \times 1000$	195	7.9	910	02:15	20
human	2-D	$9 \times 4 \times 2000$	195	2.71	880	03:00	40

5. CONCLUSIONS

Employing various spatio–temporal and bulk models for rod phototransduction, we examined the single photon response of a salamander rod photoreceptor and found parameters that produce comparable results from all the models discused here.

We also compared the responses of photoreceptors having the geometry of a salamander, a mouse and a human ROS, and saw that the thinnest (mouse) ROS produces 10 times higher response than salamander.

The results point out the usefulness of detailed spatio-temporal modeling of the phototransduction process in conducting (virtual) experiments that cannot be achieved experimentally.

REFERENCES

[1] V Alexiades, "Parameter Optimization for Biochemical Reactions in Phototransduction" to appear in *Dynamic Systems and Applications 5*, editor M.Sambandham.

[2] V Alexiades and H Khanal, "Multiphoton Response of Retinal Rod Photoreceptors", *Electronic Journal of Differential Equations*, **Conf.15**, pp.1-9, 2007.

[3] D Andreucci, P Bisegna, G Caruso, HE Hamm and E DiBenedetto, "Mathematical Model of the Spatio-Temporal Dynamics of Second Messengers in Visual Transduction", *Biophysical J.* **85**: 1358–1376, 2003.

[4] G Caruso, H Khanal, V Alexiades, F Rieke, HE Hamm, E DiBenedetto, "Mathematical and Numerical Modeling of Spatio-Temporal Signaling in Rod Phototransduction", *IEE Proc. Systems Biology*, **152**(3): 119-137, 2005.

[5] G Caruso, P Bisegna, L Shen, D Andreucci, HE Hamm, E DiBenedetto, "The Role of Incisures in Phototransduction in Vertebrate Photoreception", *Biophysical J.* **91**: 1192-1212, 2006.

[6] Carter-Dawson LD, LaVail MM. "Rods and cones in the mouse retina. I. Structural analysis using light and electron microscopy, *J Comp Neurol.* **188**(2): 245262, 1979.

[7] James T Fulton, Processes in Animal Vision (online), http://4colorvision.com/

[8] M Gray-Keller, W Denk, B Shraim and PB Detwiler, "Longitudinal Spread of Second Messenger Signals in Isolated Rod Outer Segments of Lizards", *J. Physiol.*, **519**: 679–692, 1999.

[9] RD Hamer, SC Nicholas, D Trachina, PA Liebman, and TD Lamb, "Multiple steps of phosphorylation of activated rhodopsin can account for the reproducibility of vertebrate rod single-photon response", *J. Gen. Physiol.* **122**: 419–444, 2003.

[10] H Khanal, V Alexiades, E DiBenedetto and H Hamm, "Numerical Simulation of Diffusion of Second Messengers cGMP and Ca^2+ in Rod Photoreceptor Outer Segment of Vertebrates", pp. 165-172 in *Unsolved Problems of Noise and Fluctuations in Physics, Biology and High Technology*, editor Sergey Bezrukov, American Institute of Physics, 2003.

[11] H Khanal, V Alexiades, E DiBenedetto, "Response of Dark-adapted Retinal Rod Photoreceptors", pp.138-145 in *Dynamic Systems and Applications 4*, editor M.Sambandham, Dynamic Publishers, 2004.

[12] TD Lamb and EN Pugh Jr., "A quantitative account of the activation steps involved in phototransduction in amphibian photoreceptors", *J. Physiol.* **449**: 719–758, 1992.

[13] S Nikonov, N Engheta and EN Pugh, Jr "Kinetics of Recovery of the Dark-adapted Salamander Rod Photoresponse", *J. Gen. Physiol*, **111**: 7–37, 1998.

[14] S Nikonov, TD Lamb and EN Pugh, Jr. "The Role of Steady Phosphodiestarase Activity in the Kinetics and Sensitivity of the Light-Adapted Salamander Rod Photoresponse", *J. Gen. Physiol.*, **116**: 795–824, 2000.

[15] EN Pugh, Jr. and TD Lamb, "Phototransduction in Vertebrate Rods and Cones: Molecular Mechanisms of Amplification, Recovery and Light adaptation", pp.183–255 in *Molecular Mechanism in Visual Transduction*, edited by DG Stavenga, WJ Degrip & EN Pugh Jr, Elsevier, Amsterdam, 2000.